PROCEEDINGS OF SCIENCE

High-Energy γ-rays from the Milky Way: Three-Dimensional Spatial Models for the Cosmic-Ray and Radiation Field Densities

Troy A. Porter*
W. W. Hansen Experimental Physics Laboratory and Kavli Institute for Particle Astrophysics and Cosmology, Stanford University, Stanford, CA 94305, USA E-mail:
tporter@stanford.edu

Guðlaugur Jóhannesson
Science Institute, University of Iceland, IS-107 Reykjavik, Iceland and AlbaNova Univ. Center Nordita, Roslagstullsbacken 23, SE-106 91 Stockholm, Sweden
E-mail: gudlaugu@hi.is

Igor V. Moskalenko
W. W. Hansen Experimental Physics Laboratory and Kavli Institute for Particle Astrophysics and Cosmology, Stanford University, Stanford, CA 94305, USA
E-mail: imos@stanford.edu

High-energy γ-rays of interstellar origin are produced by the interaction of cosmic-ray (CR) particles with the diffuse gas and radiation fields in the Galaxy. The main features of this emission are well understood and are reproduced by existing CR propagation models employing 2D Galactocentric cylindrically symmetrical geometry. However, the high-quality data from instruments like the *Fermi* Large Area Telescope reveal significant deviations from the model predictions on few to tens of degree scales indicating the need to include the details of the Galactic spiral structure and thus require 3D spatial modelling. In this contribution the high-energy interstellar emissions from the Galaxy are calculated using the latest release of the *GALPROP* code employing 3D spatial models for the CR source and interstellar radiation field (ISRF) densities. The interstellar emission models that include arms and bulges for the CR source and ISRF densities provide plausible physical interpretations for features found in the residual maps from high-energy γ-ray data analysis. The 3D models for CR and ISRF densities provide a more realistic basis that can be used for the interpretation of the non-thermal interstellar emissions from the Galaxy.

35th International Cosmic Ray Conference — ICRC2017
10–20 July, 2017
Bexco, Busan, Korea

*Speaker.

PoS(ICRC2017)736

1. Introduction

The high-energy γ-ray sky is dominated by the emissions produced by cosmic-ray (CR) particles interacting with matter and radiation fields in the interstellar medium (ISM) of the Milky Way. Observations of these interstellar emissions began with the OSO-III satellite in the late 1960s [1], and were followed by the space-borne experiments SAS-2 and COS-B in the early- and mid-1970s, COMPTEL and EGRET on the *Compton Gamma-Ray Observatory (CGRO)* (1990s), and the present-day *Fermi*-LAT [2]. Each of these instruments has represented a significant advance over its predecessor, with the *Fermi*-LAT providing the highest-sensitivity data so far for $\gtrsim 30$ MeV energies.

Physical modelling codes like *GALPROP* [3, 4, 5, 6] can reproduce the general features of the interstellar γ-ray emission over the whole sky, showing that the CR physics and interactions producing it are well-understood. However, it is the residuals from when interstellar emission models (IEMs) are subtracted from the data that provide the potential for identifying new phenomena in high-energy γ-rays. Their understanding requires a careful assessment of the the modelling inputs, in particular those related to the CR source and ISM densities.

To date the most extensive study of high-energy IEMs has been made by the *Fermi*–LAT team [7] using a grid of 128 *a-priori GALPROP* models normalised to reproduce local CR data. The grid entries are categorised by 4 CR source spatial density models from the literature (supernova remnants, 2 pulsar, and OB-stars), multiple CR propagation halo sizes, and other parameters related to the interstellar gas. These IEMs employ a 2D Galactocentric cylindrically symmetric spatial geometry, which has been the norm since the *CGRO*-era due to the limited quality of the γ-ray data, information on ISM distributions, and computing resources available. Examination of the residual maps developed in that work shows ∼few to tens of degrees scale features that are asymmetric about the meridian defined by Galactic longitude $l = 0^\circ$ and the Galactic plane. Some of them are likely related to large-scale structure in the CR and ISM distributions that are not properly accounted for by the 2D-based IEMs. Another notable analysis is the *Fermi*–LAT team investigation of the γ-ray emission toward the inner Galaxy [8], which uses a subset of the 128–model grid as baseline IEMs to develop estimates for the fore/background from the Galaxy, and enable extraction of the γ-ray emission from within ~ 1 kpc about the Galactic centre (GC). An attempt to compensate for the modelling limitations of the 2D IEMs is made in that work by introducing new degrees of freedom for the inverse Compton (IC) component and fitting the γ-ray emission outside of a $15^\circ \times 15^\circ$ region about the GC to estimate the fore/background. An interesting result found from the application of the procedure developed in [8] is that for Galactocentric radii $R \sim 3-8$ kpc the baseline IEM predictions need to be scaled upward by $\sim 20-25\%$ to account for the positive residuals for Galactic longitudes $15^\circ \lesssim |l| \lesssim 80^\circ$. In addition, they found that the IC emission in and about the GC over the $15^\circ \times 15^\circ$ is strongly dominant compared to that related to CRs interacting with the gas. These somewhat puzzling results are difficult to further interpret using the 2D-based IEMs. The larger parameter space afforded by 3D IEMs is a logical next step in the evolution of physics-based modelling of the high-energy emissions from the Galaxy.

The *GALPROP* code has been capable of 3D CR propagation calculations since the beginning [4, 9, 10] but this mode has had limited usage because of the available data quality and computing resources necessary. Even the current data and theory does not provide for a complete 3D model

of the ISM to be built. Thus, studying the effects of 3D structures on various observables is still at its early stages.

High-energy interstellar emission calculations in 3D have been described by [11, 12] using *GALPROP*, and [13] with the *PICARD* code, where the former has considered both 3D CR source and gas density models, while the latter uses a spiral arm model for the CR source densities but 2D models for the ISM densities. So far 3D interstellar radiation field (ISRF) models have not been employed, which are necessary for comprehensive treatment of the CR electrons and positrons and their high-energy emissions.

In this contribution, a study is made of the high-energy interstellar emissions calculated using 3D models for the CR source and ISRF densities in the Galaxy. Three CR source density models are considered that have the injected CR power distributed as a mixture of an axisymmetric smooth disc and/or spiral arms. Two 3D ISRF models termed R12 and F98 that are described elsewhere [14] are developed and their Galaxy-wide spectral intensity distributions are calculated. The new release of the *GALPROP* code [15] is employed using these CR and ISRF density models as inputs for the CR propagation and high-energy interstellar emission calculations. With the addition of a population of CR sources distributed according to the stellar bulge/bars of either of the R12 and F98 ISRF models, the models with spiral arms provide a plausible physical explanation for the puzzling results from the analysis of high-energy γ-ray toward the inner Galaxy obtained by the *Fermi*–LAT team in [8].

2. Calculations and Results

The focus in this work is on the CR induced γ-ray emission from different realisations of the CR source and ISRF distributions. The propagation model is therefore limited to diffusive re-acceleration with an isotropic and homogeneous diffusion coefficient that has a power-law dependence with rigidity. The CR injection spectra are modelled as rigidity-dependent broken power laws[1] with parameters derived as by a recent study [16]. Electrons, protons, and He each have two breaks while elements with $Z > 2$ are modelled with a single break. The extra break for the low-mass elements is to model the spectral change observed at rigidities above 100 GV [17, 18]. The CR source density model is 100% disc (2D), 50%/50% disc/spiral arm, or 100% spiral arm, where the disc and arms have the same exponential scale-height (200 pc) perpendicular to the Galactic plane. The smooth disc spatial density follows the radial distribution of pulsars as given by [19]. The spiral arm spatial density follows that of the 4 major arms in the R12 model [14] and assumes an identical injection of CR power by each arm. The CR source density models are termed SA0, SA50, and SA100, following the proportion of injected CR luminosity by the spiral arms. The normalisation for the injected CR power in each is obtained by requiring the propagated CR intensities agree with the local CR observations[2], where all calculations use the IAU recommended Sun-GC distance of $R_S = 8.5$ kpc [20].

For each of the SA0, SA50, and SA100 CR source densities the propagation model parameter tuning is made using a maximum-likelihood fit employing data from AMS–02 [21, 18, 17, 22],

[1] Parameterisation: $q(R) \propto R^{\gamma_0}$ for $R < R_1$, $q(R) \propto R^{\gamma_1}$ for $R_1 < R < R_2$, and $q(r) \propto R^{\gamma_2}$ for $R > R_2$.

[2] The proton and e^- flux is normalised at the Solar location at a kinetic energy of 100 GeV.

HEAO3-C2 [23], Voyager-1 [24], and PAMELA [25]. To reduce the number of parameters in each fit the procedure is split into two stages, similar to the analysis described by [24]. The propagation model parameters that are fit for are the diffusion coefficient normalisation and rigidity dependence, Alfvén velocity, normalisations and rigidity dependencies of CR species, and force-field modulation potentials. There is a strong degeneracy between the halo height and the normalisation of the diffusion coefficient. Even though using radio-nuclei (^{10}Be, ^{26}Al, ^{36}Cl, ^{54}Mn) constrains the halo size significantly the range of possible values remains quite wide. Instead of fitting for both simultaneously, the halo height is set to 6 kpc, in good agreement with previous analyses [26, 16]. The first stage of the procedure fits for the other propagation model parameters together with the injection spectra and abundances of $Z > 2$ elements. With the propagation parameters and the injection spectra for $Z > 2$ determined, they are held constant. The injection spectra for electrons, protons, and He are then obtained in the second stage of the procedure. To reduce the number of parameters the injection spectrum of He is coupled with that of the protons such that the location of the breaks are the same, and all the indices are smaller by a value Δ_{He} that is a parameter in the fit procedure. This is similar to the linking of the proton and He spectra for the analysis described by [16]. Fourteen parameters are determined by the first stage of the procedure, while the second stage fits for fifteen parameter values.

The calculations are made for a Cartesian spatial grid with dimensions $\pm$20 kpc for the X and Y coordinates, with $\Delta X,Y,Z = 0.125$ kpc and CR kinetic energy grid covering 10 MeV/nucleon to 1 TeV/nucleon with logarithmic spacing at 10 bins/decade. The span and sampling of the spatial and energy grids is chosen to enable realistic and efficient computations given the available resources. The spatial grid sub-division size allows adequate sampling of the CR and ISM density distributions. The X,Y size of the grid is sufficient to ensure that CR leakage from the Galaxy is determined by the size of the confinement region perpendicular to the Galactic plane at the Solar system location where the propagation model parameters are fitted.

Full results of the fitting procedure are given in a forthcoming paper (Porter et al., in press) but it is sufficient to note that the calculated CR spectra for all source density models are within $\sim 5\%$ of each other, and agree well with the data and are generally well within the data uncertainties.

High-energy interstellar emissions are calculated using *GALPROP* for the SA0, SA50, and SA100 source density models, and the standard 2D [7] and R12/F98 3D ISRF models. The γ-rays are calculated from 1 MeV to 100 GeV energies using a logarithmic energy grid with 10 bins/decade spacing. Higher γ-ray energies correspond to CRs with energies $\gtrsim 1$ TeV where the steady-state source injection paradigm employed in this paper is less valid [10]. All calculations of the IC contribution use the anisotropic scattering cross section [28] that accounts for the full directional intensity distribution for each of the Std, R12, and F98 models. The SA0 CR source density and Std ISRF (SA0–Std) is used as the reference case. This combination corresponds to the 2D CR source and ISRF density scenario that has been the standard approach for interstellar emission modelling in the past.

As an example, Fig. 1 (left) shows the fractional residual map[3] obtained for the SA100–R12 (CR–ISRF) model combination for a γ-ray energy of 1.2 GeV. Toward the inner Galaxy a doughnut-like feature with excess emission concentrated near $l \sim \pm 45^\circ$ and extending to high latitudes is

[3] $(model - ref)/ref$ where ref is the SA0–Std reference combination.

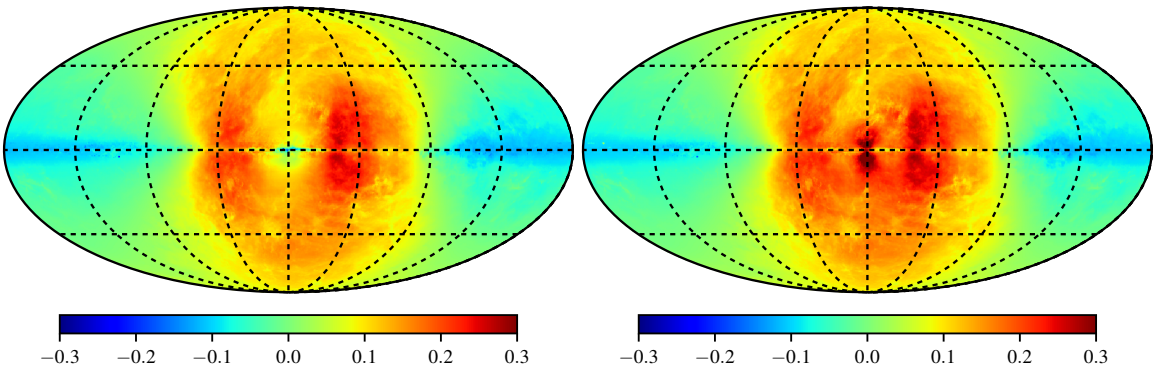

Figure 1 Fractional residual map at 1.2 GeV for the SA100–R12 (left) and SA100/R12B–R12 (right) CR source and ISRF density model combinations with respect to the SA0–Std reference case. The map is in Galactic coordinates with $l, b = 0^\circ, 0^\circ$ at the centre. The longitude meridians and latitude parallels have 45° spacing.

evident. This is caused by the combined emissions from CR nuclei and electrons interacting with the relatively nearby gas ($\sim 100 - 500$ pc) and the pile-up of the IC emissions from nearby and farther along the line-of-sight. For the gas-related emissions there are higher CR densities in the ISM due to their localised injection in the arms, which illuminate the gas that is nearby to these regions differently to the CR densities produced for the SA0 model. Enhanced IC emissions result from higher CR lepton densities and ISRF intensities in and about the arms for the SA100 CR and R12 ISRF density models, respectively.

Comparison of the residual maps with those derived from high-energy γ-ray analysis, such as in Fig. 2 of [8] that uses the (2D) SA0–Std combination as its baseline IEM, show similar spatial excesses at a level $\gtrsim 30\%$ that extend out of the plane for $-45^\circ < l < 45^\circ$. These are somewhat higher but similar in spatial distribution to those shown in Fig. 1 (left) where there are peaks near $l \sim 45^\circ$ and $l \sim -30^\circ$ corresponding to the spiral arm enhancements together with a general in-fill up to $|b| \sim 45^\circ$ latitudes. However, Fig. 1 (left) has a central 'hole' about the GC caused by the lower CR energy density in that region, whereas the residuals shown in Fig. 2 of [8] are $\gtrsim 30 - 40\%$. A resolution to obtain comparable residual excesses that in-fill the region about the GC for the SA100 models is to introduce an extra source density model that provides additional CR power there. An explanation for such an additional component is that it could be a bulge/bar-related population of CR accelerators that injects both nuclei and leptons, or possibly only leptons. The first possibility is examined by recalculating the interstellar emissions with an additional CR central source density distribution following the R12/F98 stellar bulge/bar but with CR injection abundances the same as the arms for the SA100 density model. The fractional residual for this 'what-if' scenario for the R12 bulge (termed SA100/R12B–R12) is shown for a γ-ray energy 1.2 GeV in Fig. 1 (right) where the corresponding injected CR power is $\sim 1/25$ of that from the CR arms. The residuals are $\sim 50\%$ of the maximum of those from [8] so possibly a higher injected CR power is required. But no further tuning of the model parameters is made here; detailed optimisations to determine the correct normalisation and spatial morphology require

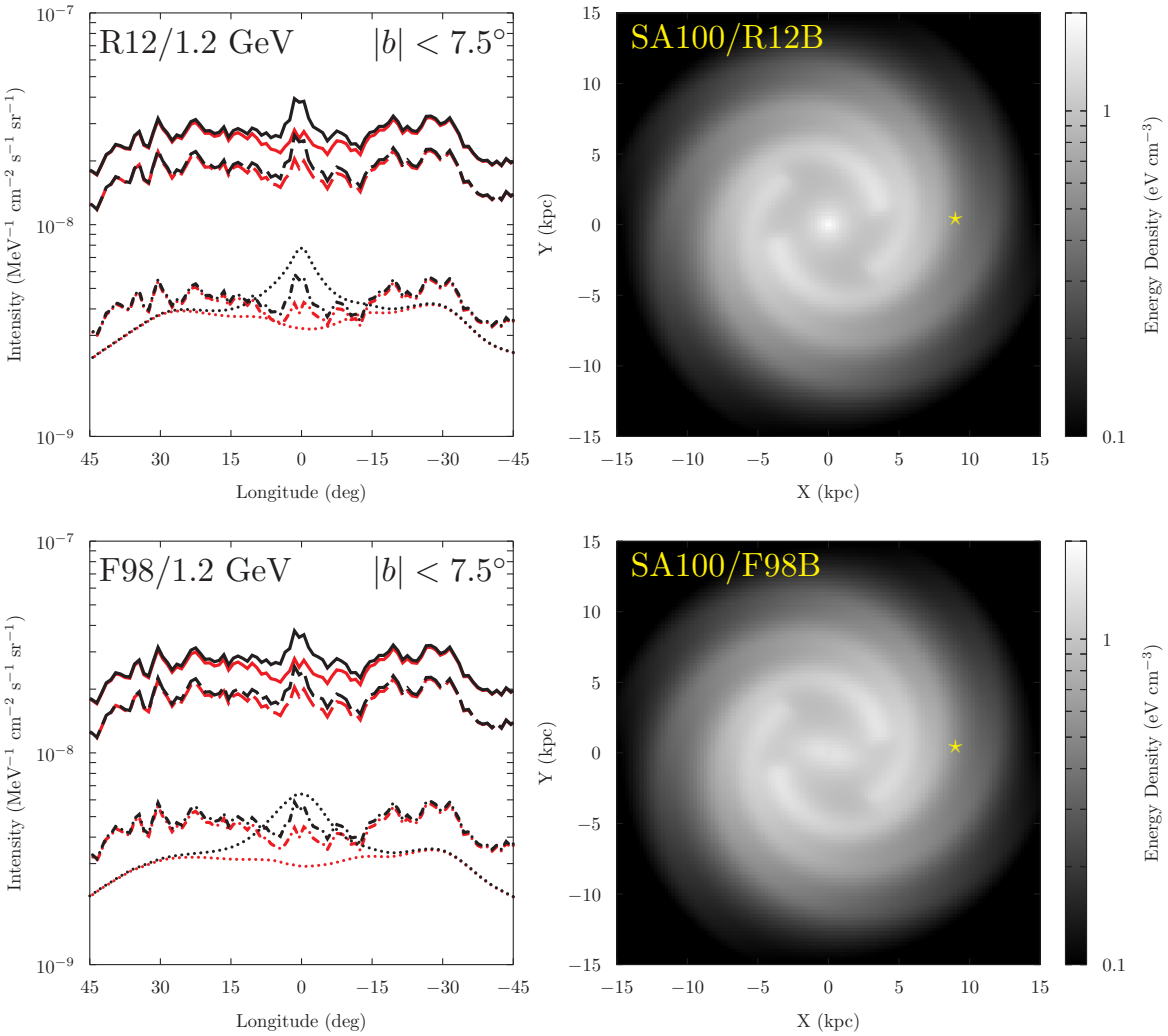

Figure 2 Left panel: longitude profile for the intensity at 1.2 GeV averaged over $-7.5° \leq b \leq 7.5°$. Top shows the SA100–R12 combination (red lines) and SA100/R12B–R12 combination (black lines). Bottom shows the SA100-F98 combination (red lines) and SA100/F98B–F98 combination (black lines). Line-styles: solid, total; long-dashed, π^0-decay; dash-dot, Bremsstrahlung; dotted, IC. Right panel: spatial distribution of integrated CR energy density at the Galactic plane for the SA100/R12B (top) and SA100/F98B (bottom) CR source density models. The yellow star shows the location of the Solar system.

fitting to γ-ray data, which will be the subject of subsequent work.

Figure 2 (left) shows the longitude profiles toward the inner Galaxy for the SA100/R12B–R12 (top) and SA100/F98B–F98 (bottom) model combinations, and Fig. 2 (right) shows the corresponding CR energy density distributions in the ISM. These provide a framework for interpreting the results of [8]. For the inner $R \lesssim 3$ kpc, the CRs injected by the bulge/bar in combination with the high ISRF spectral intensities over the region for the R12/F98 ISRF models result in a much higher IC intensity compared to the SA0–Std reference case. The multiplier effect enhances the IC by factors $\sim 2-3$, which is similar to the factor ~ 4 found by [8]. For $R \sim 3-8$ kpc, the propaga-

tion smoothes the CRs injected by the arms into a quasi-axisymmetric ring (Fig. 2, right). The CR energy densities over the region are $\sim 20-30\%$ higher compared to the SA0 source model, which is similar to the scaling factors found also in the *Fermi*–LAT study.

This work has demonstrated the need for detailed modelling of the distribution of CR sources and the ISRF taking into account the 3D structure of the ISM. The residual structure in the calculated maps resemble features that have been previously interpreted as possible signs of new physics. However, further work is needed to optimise the models and more carefully tune them to the available data.

Acknowledgments

FRaNKIE and *GALPROP* development is partially funded via NASA grants NNX13AC47G and NNX17AB48G. Some of the results in this paper have been derived using the HEALPix [29] package.

References

[1] W. L. Kraushaar et al., *High-Energy Cosmic Gamma-Ray Observations from the OSO-3 Satellite*, *ApJ* **177** (Nov., 1972) 341.

[2] W. B. Atwood et al., *The Large Area Telescope on the Fermi Gamma-Ray Space Telescope Mission*, *ApJ* **697** (June, 2009) 1071–1102, [arXiv:0902.1089].

[3] I. V. Moskalenko and A. W. Strong, *Production and Propagation of Cosmic-Ray Positrons and Electrons*, *ApJ* **493** (Jan., 1998) 694–707, [astro-ph/9710124].

[4] A. W. Strong and I. V. Moskalenko, *Propagation of Cosmic-Ray Nucleons in the Galaxy*, *ApJ* **509** (Dec., 1998) 212–228, [astro-ph/9807150].

[5] A. W. Strong, I. V. Moskalenko, and O. Reimer, *Diffuse Continuum Gamma Rays from the Galaxy*, *ApJ* **537** (July, 2000) 763–784, [astro-ph/9811296].

[6] A. E. Vladimirov et al., *GALPROP WebRun: An internet-based service for calculating galactic cosmic ray propagation and associated photon emissions*, *Computer Physics Communications* **182** (May, 2011) 1156–1161, [arXiv:1008.3642].

[7] M. Ackermann et al., *Fermi-LAT Observations of the Diffuse γ-Ray Emission: Implications for Cosmic Rays and the Interstellar Medium*, *ApJ* **750** (May, 2012) 3, [arXiv:1202.4039].

[8] M. Ajello et al., *Fermi-LAT Observations of High-Energy Gamma-Ray Emission toward the Galactic Center*, *ApJ* **819** (Mar., 2016) 44.

[9] A. W. Strong and I. V. Moskalenko, *SNR and fluctuations in the diffuse Galactic γ-ray continuum*, in *Gamma 2001: Gamma-Ray Astrophysics* (S. Ritz, N. Gehrels, and C. R. Shrader, eds.), vol. 587 of *American Institute of Physics Conference Series*, pp. 533–537, Oct., 2001.

[10] A. W. Strong and I. V. Moskalenko, *A 3D time-dependent model for Galactic cosmic rays and gamma rays*, *International Cosmic Ray Conference* **5** (Aug., 2001) 1964–1967, [astro-ph/0106505].

[11] G. Johannesson, I. V. Moskalenko, and T. Porter, *Toward 3D mapping of the interstellar medium in the Milky Way: impact on cosmic rays and diffuse emission*, *Br. J. of Phys.* **ICRC2013** (2013) 0913.

[12] G. Johannesson et al., *The Effects of Three Dimensional Structures on Cosmic-Ray Propagation and Interstellar Emissions*, *PoS* **ICRC2015** (2016) 517.

[13] R. Kissmann et al., *Diffuse Gamma Rays in 3D Galactic Cosmic-ray Propagation Models*, *ArXiv e-prints* (Jan., 2017) [arXiv:1701.0728].

[14] T. A. Porter, G. Johannesson, and I. V. Moskalenko, *The Interstellar Radiation Field of the Milky Way in Three Spatial Dimensions*, *These Proceedings* (July, 2017).

[15] I. V. Moskalenko et al., *GALPROP Code for Galactic Cosmic Ray Propagation and Associated Photon Emissions*, *These Proceedings* (July, 2017).

[16] G. Jóhannesson et al., *Bayesian Analysis of Cosmic Ray Propagation: Evidence against Homogeneous Diffusion*, *ApJ* **824** (June, 2016) 16, [arXiv:1602.0224].

[17] M. Aguilar et al., *Precision Measurement of the Proton Flux in Primary Cosmic Rays from Rigidity 1 GV to 1.8 TV with the Alpha Magnetic Spectrometer on the International Space Station*, *Physical Review Letters* **114** (May, 2015) 171103.

[18] M. Aguilar et al., *Electron and Positron Fluxes in Primary Cosmic Rays Measured with the Alpha Magnetic Spectrometer on the International Space Station*, *Physical Review Letters* **113** (Sept., 2014) 121102.

[19] I. Yusifov and I. Küçük, *Revisiting the radial distribution of pulsars in the Galaxy*, *A&A* **422** (Aug., 2004) 545–553, [astro-ph/0405559].

[20] F. J. Kerr and D. Lynden-Bell, *Review of galactic constants*, *MNRAS* **221** (Aug., 1986) 1023–1038.

[21] M. Aguilar et al., *Precision Measurement of the Boron to Carbon Flux Ratio in Cosmic Rays from 1.9 GV to 2.6 TV with the Alpha Magnetic Spectrometer on the International Space Station*, *Physical Review Letters* **117** (Dec., 2016) 231102.

[22] M. Aguilar et al., *Precision Measurement of the Helium Flux in Primary Cosmic Rays of Rigidities 1.9 GV to 3 TV with the Alpha Magnetic Spectrometer on the International Space Station*, *Physical Review Letters* **115** (Nov., 2015) 211101.

[23] J. J. Engelmann et al., *Charge composition and energy spectra of cosmic-ray nuclei for elements from Be to NI - Results from HEAO-3-C2*, *A&A* **233** (July, 1990) 96–111.

[24] A. C. Cummings et al., *Galactic Cosmic Rays in the Local Interstellar Medium: Voyager 1 Observations and Model Results*, *ApJ* **831** (Nov., 2016) 18.

[25] O. Adriani et al., *Measurement of Boron and Carbon Fluxes in Cosmic Rays with the PAMELA Experiment*, *ApJ* **791** (Aug., 2014) 93, [arXiv:1407.1657].

[26] I. V. Moskalenko, A. W. Strong, and S. G. Mashnik, *Propagation of Cosmic Rays: Nuclear Physics in Cosmic-Ray Studies*, in *International Conference on Nuclear Data for Science and Technology* (R. C. Haight, M. B. Chadwick, T. Kawano, and P. Talou, eds.), vol. 769 of *American Institute of Physics Conference Series*, pp. 1612–1617, May, 2005. astro-ph/0411400.

[27] T. A. Porter et al., *Inverse Compton Origin of the Hard X-Ray and Soft Gamma-Ray Emission from the Galactic Ridge*, *ApJ* **682** (July, 2008) 400–407, [arXiv:0804.1774].

[28] I. V. Moskalenko and A. W. Strong, *Anisotropic Inverse Compton Scattering in the Galaxy*, *ApJ* **528** (Jan., 2000) 357–367, [astro-ph/9811284].

[29] K. M. Górski et al., *HEALPix: A Framework for High-Resolution Discretization and Fast Analysis of Data Distributed on the Sphere*, *ApJ* **622** (Apr., 2005) 759–771, [astro-ph/0409513].